Acta Polytechnica **64**(4):385–397, 2024
https://doi.org/10.14311/AP.2024.64.0385

Published by the Czech Technical University in Prague

INVESTIGATION THE PLASTIC FLOWS IN THE METAL STAMPING-DRAWING PROCESS AT THE DIE CORNER

Anton V. Onopchenko[a], Maksym O. Kurin[a,*], Yurii V. Shyrokyi[b], Oleksii O. Horbachov[a]

[a] *National Aerospace University "Kharkiv Aviation Institute", Faculty of Aviation Engines, Technologe of Manufacturing Aviation Engines Department, Vadyma Manka 17, 61070 Kharkiv, Ukraine*

[b] *National Aerospace University "Kharkiv Aviation Institute", Faculty of Aviation Engines, Theoretical Mechanics, Mechanical Engineering, and Robotic Systems Department, Vadyma Manka 17, 61070 Kharkiv, Ukraine*

[*] corresponding author: m.kurin@khai.edu

Abstract. The present investigation covers the study of the influence of metal-plastic flow on the die corner for the deformed state of the blank and energy-power parameters during stamping-drawing. The influence of workpiece size and material on stress intensity and maximum deformation force has also been investigated both experimentally and theoretically. In addition, simulation of the stamping and drawing process was also presented. One type of die, with variations in diameter are considered different in the drawn part size and for each standard size four types of workpiece materials have been considered. The stamping process continued until the part failed structurally. The predicted test results show a dependence of the maximum load and stress intensity on both the diameter of the blank and the yield strength of the alloys and these data are in agreement with the actual measured values. Then, the method for calculating the processes of plastic deformation of metals based on a closed set of equations of continuum mechanics is proposed for the theoretical study of energy-power parameters of the technological processes. Comparison of the results of a full-scale experiment, simulation of metal flow at the die corner and theoretical calculations shows that the proposed theoretical model gives satisfactory results and can be effectively used for engineering calculations.

Keywords: Sheet metal stamping-drawing, plastic flows, modelling, deformation intensity, stress intensity, process power parameters.

1. Introduction

Modelling the processes involved in the mechanical machining of parts has an undeniable number of advantages [1, 2] over full-scale experiments. This makes it possible to significantly simplify the technological preparation of production, and to correct theoretical models of various processes [3]. Using modern software systems, such as Abaqus, Simufact Forming, LS-DYNA and others, makes it possible to obtain a significant data array that simplifies the analysis of processes [4, 5], with the ability to quickly adjust input parameters in order to obtain optimal product characteristics, bypassing the laborious and expensive practical experiments. In addition, the use of such systems makes it possible to refine and verify the developed theoretical models using limited field and experimental data [6, 7]. In addition, simulation methods could be implemented for modelling of new technologies [8].

It is known that 60–70 % of the aircraft total volume is made by blanking and stamping operations [9]. In general, using stronger materials and thinner sheets can significantly improve the operational reliability and performance characteristics of aircrafts and engines in aviation technology [10]. Stamping-drawing is a common punching operation in mechanical engineering [11] designed to produce hollow parts and workpieces of various shapes and sizes. In most cases, stamping-drawing can be used to produce parts of complex geometry from a sheet metal blank, with strength, rigidity, and specific weight being slightly better than that of assemblies produced by riveting and welding.

There is currently a trend to improve stamping processes, tools and equipment. In fact, there has been a lot of work done to investigate the most important factors that affect the stamping-drawing process, such as lubrication [12] and coefficient of friction [13], die corner radius [14], punch corner radius [15], punch force [16], material properties [17], material thickness [18], blank size [19], punch and die edges [20], punch speed [21]. In our opinion, the reviewed works do not pay due attention to the die corner and its influence on the performance parameters of the stamping-drawing process. As we know, at the corner of the die the transition from the flange to the wall blank occurs and the stress-strain state changes. This has a significant effect [22] on such important parameters of the drawing process as stress in the material, drawing force, wrinkle formation [23], thinning of the wall material, limiting draw ratio, and matrix durabil-

ity [24]. However, the authors use simplified formulae to calculate the components of deformations, stresses and tensile forces [25, 26]. Typically, these equations do not fully correspond to the physics of metal-plastic flow at the die corner and cannot be used to construct and analyse such important characteristics as strain components, strain rates, strain intensities and strain rates, and integral characteristics such as stress intensity. Therefore, we are to draw a conclusion on methods for determining the deformed state of the blank and energy-power parameters during stamping-drawing do not fully describe the actual state of the process.

The main objective of this paper is to improve the methodology for calculating energy-power characteristics of the drawing–stamping process, taking into account the metal deformation zone at the die corner. In this article, we focus on a method for calculating the parameters of plastic deformation of metals at the die corner, based on a closed system continuum mechanics equations. As a result, we have obtained analytical expressions for the calculation components of strain rates, strains and their intensities at the die corner. This paper presents a new approach to calculate stress intensity, an important characteristic for calculating the drawing force during stamping-drawing. The proposed method validated using the finite elements method by comparison with theoretical demonstration. This result will serve as a basis for a future optimisation of quick and easy calculation of the stress-strain state of the blank and drawing forces.

2. Numerical simulation of the stamping-drawing in LS-DYNA

In order to test the effectiveness of the model for calculating the processes of plastic deformation of different sheet materials, based on a closed set of equations of continuum mechanics, in predicting the numerical simulation of sheet metal stamping-drawing, the model established in this paper was used to simulate the distribution of plastic equivalent stresses in sheet metal parts, based on LS-DYNA software. Package LS-DYNA version R11.2.2 (revision R11.2-290-g768d145fcb) software was used to simulate the stamping-drawing process of the alloys sheets.

One type of die, with variations in diameters are considered differing, in the drawn part size and for each standard size four types of blank materials have been considered.

2.1. Geometric models

The three-dimensional models, including punch, die, blank holder, and blank, were modelled using SOLID software and then exported to LS-DYNA software. Due to the symmetry, the numerical analysis of the stamping-drawing process was performed using only one quarter of the 3D numerical model to reduce the computational time.

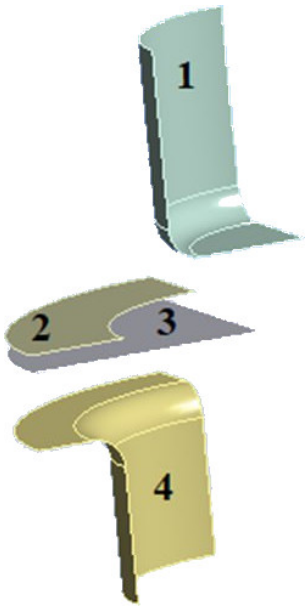

Figure 1. Numerical modelling of stamping-drawing: 1 – Punch, 2 – blank holder, 3 – blank, 4 – draw cavity.

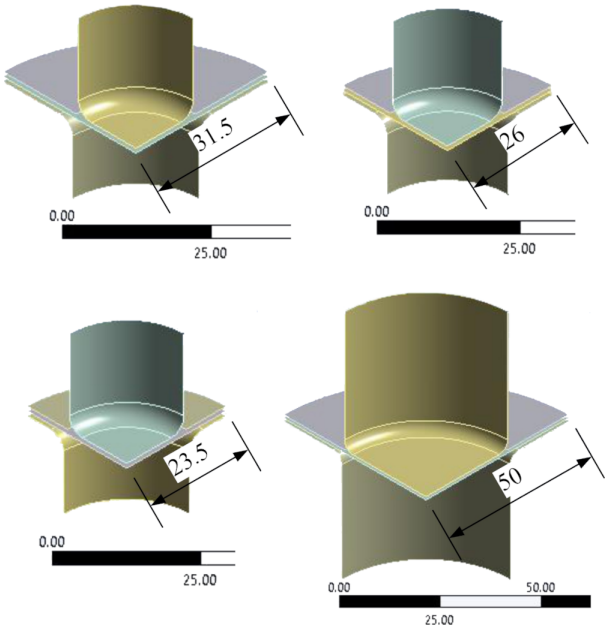

Figure 2. Investigated models.

The numerical model of LS-DYNA parts forming the simulation is shown in Figure 1.

The four types of drawing die assembly are shown in Figure 2 for different workpieces diameters (47 mm, 52 mm, 63 mm and 100 mm) with the same thickness of 1 mm.

In order to obtain reliable results from the numerical modelling of stamping-drawing, sheet metal simulations are necessary to ensure automatic contact pairs during the solution, i.e. to provide clearances between some parts in the initial position. Therefore, the blank is raised 0.5 mm above the die cavity, but the blank holder and punch are higher (at 1 mm).

Material grade	Young's modulus [GPa]	Yield strength [MPa]	Tensile strength [MPa]	Elongation [%]
OT4	115	550...660	700...900	15...25
D16T	72	300...320	440...460	10...17
AMc	71	60...130	110...170	10...25
AMg	71	120...150	230...300	20...25

TABLE 1. Workpiece material properties.

Material	Si	Mg	Mn	Fe	Cu	Cr	Zn	Zr	Ti	Al
OT4	≤ 0.12	-	$0.8 \div 2$	≤ 0.3	-	-	-	≤ 0.3	rest	$3.5 \div 5$
D16T	≤ 0.5	$1.5 \div 1.8$	$0.3 \div 0.9$	≤ 0.5	$3.8 \div 4.9$	≤ 0.1	≤ 0.25	-	≤ 0.15	rest
AMc	≤ 0.6	≤ 0.2	$1 \div 1.6$	≤ 0.7	≤ 0.1	-	≤ 0.1	-	≤ 0.2	rest
AMg	≤ 0.5	≤ 6	$0.5 \div 0.8$	≤ 0.5	≤ 0.2	-	≤ 0.2	-	$0.02 \div 0.1$	rest

TABLE 2. Chemical composition of the materials according to the supplier's specifications in wt%.

2.2. MATERIALS

The punch, die, and blank holder were defined as discrete, absolutely rigid bodies, corresponding to the assignment of material ∗MAT_020 from the LS-DYNA material library [27].

In addition, the workpiece was defined as a deformable body and material properties were selected from the GRANTA material database [28].

As is well known, when performing finite element simulations of sheet metal forming operations at room temperature, the flow curve of the sheet metal tested at a standard strain rate is usually used even though the strain rate is different in different regions of the drawn part and varies over a wide range for a given punch speed [29, 30]. For this, a material with a given set of properties was sought, as shown in Table 1. The chemical composition of the aluminium and titanium alloys are summarised in Subsection 3.1, Table 2.

As a result, four analogues of these materials were identified, which were preferred for numerical modelling of parts by stamping-drawing because there are no special material requirements. These materials also have complete diagrams of true stresses ϵ versus true (logarithmic) strains σ, which are shown in Figure 3. To define a material in LS-DYNA, the ∗MAT_PIECEWISE_LINEAR_PLASTICITY (∗MAT_24) model have been used, where the ϵ-σ diagrams are directly specified. The deformations corresponding to the material failure are accepted from Table 1 (upper limits).

2.3. CONTACT AND SYMMETRY

The part contacts with the rigid punch, draw cavity, and blank holder have been modelled using the ∗CONT_FORMING_SURFACE_TO_SURF type penalty-based contacts (Pure Penalty). In this contact algorithm, only the penetration from the slave surface is checked, and the penetration from the master side is not taken into account, it makes the computational algorithm more efficient. The thickness of the metal, which was used to determination contact pairs, was to 1 mm for the part (real dimension), and equal to zero for die elements.

In a numerical simulation of sheet metal forming, classical Coulomb's law is commonly used to describe the friction characteristics and thus, this model of friction between the blank and die parts has been adopted. The friction coefficient between the steel die parts and sheet was set to 0.3 for titanium and 0.18 for aluminium alloys, based on a previous tribological experimental studies that conducted simulations of the forming and drawability under different process conditions for aluminium [31, 32] and titanium alloys [32–34] respectively.

Furthermore, the influence of the coefficient of friction on the potential stamping-drawing depth of the part has been investigated with a numerical experiment for a titanium part with a diameter of 47 mm, the results of which are shown in Figure 4.

According to the simulation results of the friction impact, the critical major region extends between the friction coefficients of 0–0.1, with a further increase leading to a minor reduction of the drawing depth. For reference, the nodal edges of an empty quarter were given the conditions of plane symmetry with respect to the x-z and y-z planes.

2.4. FINITE ELEMENT MODEL

A four-node shell element is proposed in a blank geometric model for the calculation in which the Belytschko-Tsay model is used with a variable thickness. In the Gauss integration method, which is applied through the thickness, the integration is performed at ten points.

To determine the finite element mesh size, the deformation process of a circular titanium blank (47 mm diameter) was calculated with element sizes of 2 mm, 1.5 mm, 1 mm and 0.5 mm; with an adaptive finite element mesh, the element size was modified and reduced to 0.25 mm. As before, the maximum drawing depth of the workpiece was a controlled parameter (results are shown in Table 3 and Figure 5). Hence,

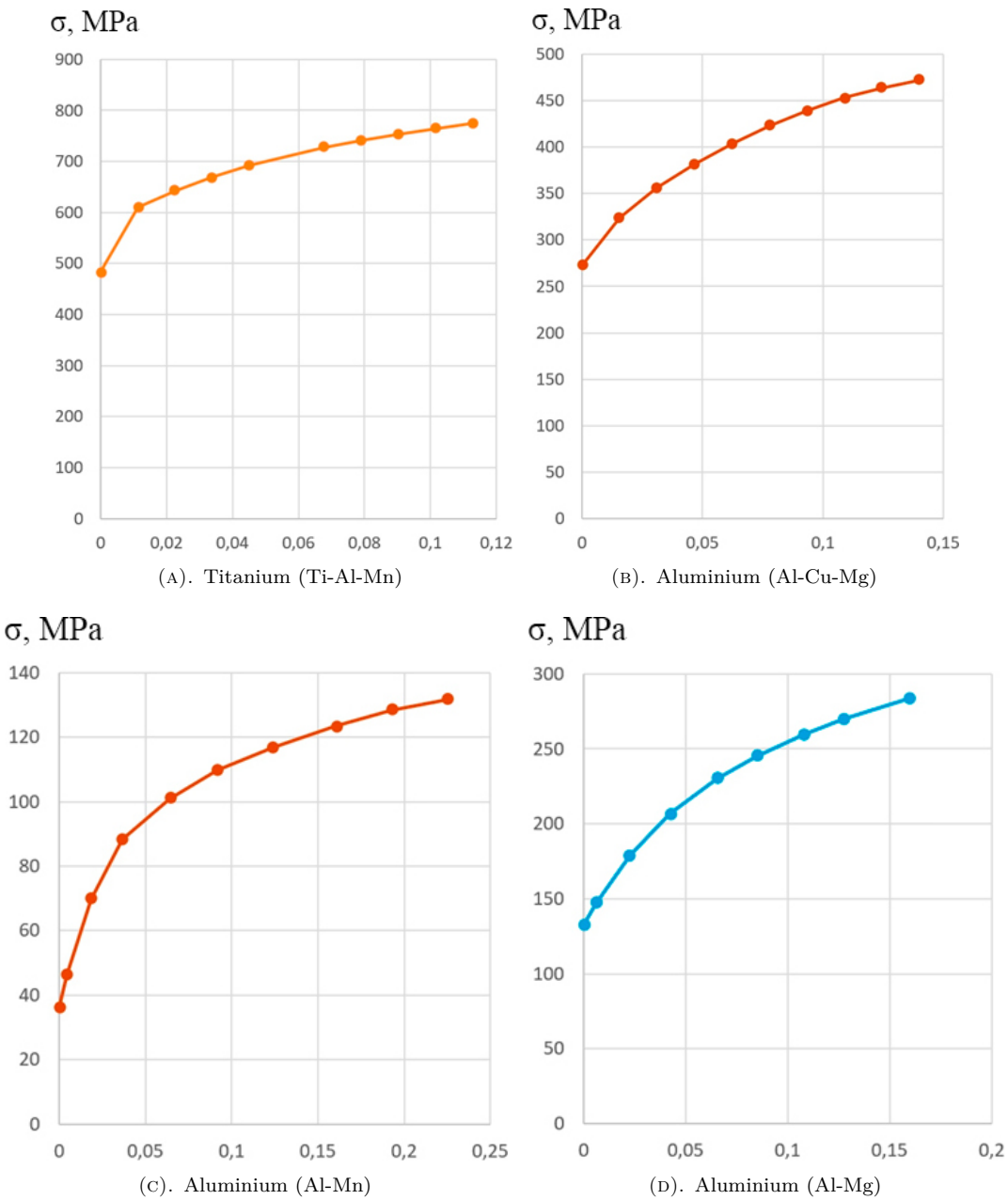

(A). Titanium (Ti-Al-Mn)

(B). Aluminium (Al-Cu-Mg)

(C). Aluminium (Al-Mn)

(D). Aluminium (Al-Mg)

Figure 3. Diagrams σ-ϵ s for the used materials.

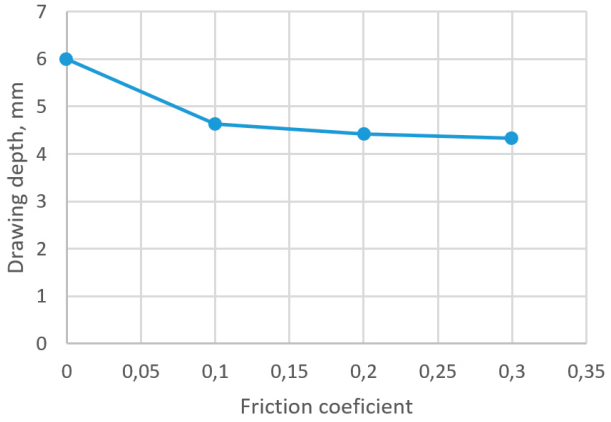

Figure 4. Drawing depth for different coefficents of friction.

Finite element size [mm]	Draw depth [mm]	Error [%]
2	5.14	6.49
1.5	4.54	17.44
1	5.77	4.92
0.5	5.47	0.41
0.25 (adaptive grid)	5.50	-

Table 3. Effect of finite element mesh size on draw depth.

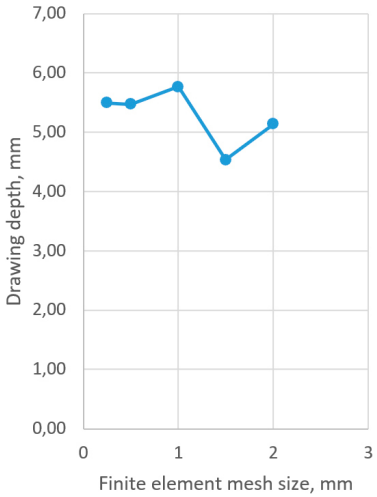

(A). Drawing depth for different mesh size.

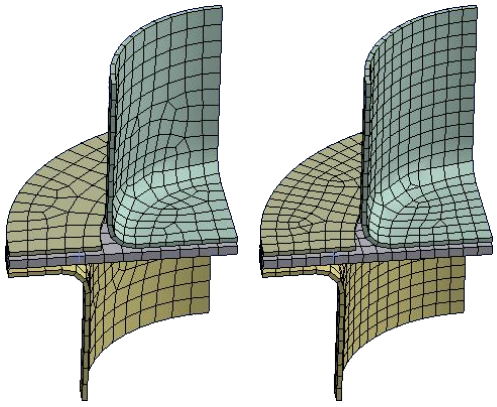

(B). 2 mm. (C). 1.5 mm.

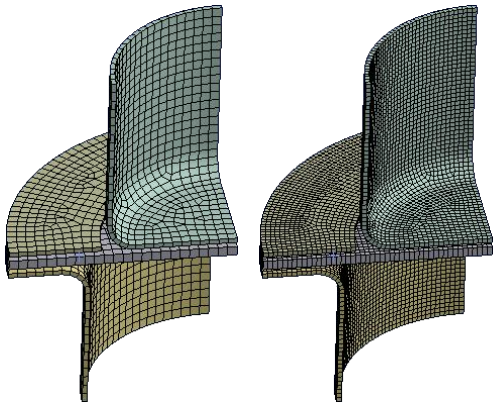

(D). 1 mm. (E). 0.5 mm.

FIGURE 5. Maximum drawing depth for various final element size.

a model with an element size of 1 mm will give us an error that does not exceed the engineering accuracy of 5 %; therefore, a finite element mesh with a cell size of 1 mm has been used in all calculations.

Such discrepancies are explained by the chosen Gaussian integration method for the 10 control points in the LS-DYNA calculation package, which is the most accurate of this problem.

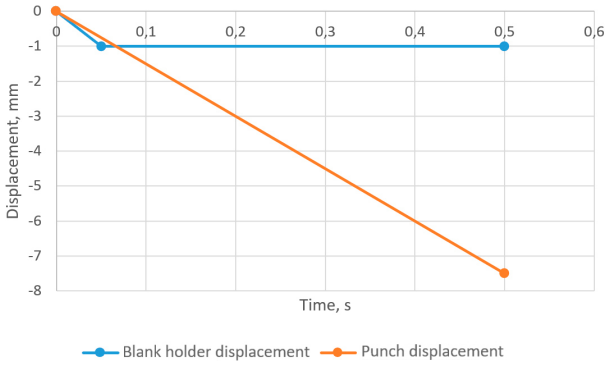

FIGURE 6. Blank holder and punch displacements.

2.5. LS-DYNA SOLVER SETTINGS, CONSTRAINING AND LOADING THE MODEL

Since no dynamic hardening was specified in material properties, the strain rate was not taken into account, and punch speed was increased to an average of $15\,\mathrm{mm\,s^{-1}}$, which is low in terms of kinetic energy. These results have been validated by the numerical experiment (a calculation was carried out at a speed of $3\,\mathrm{mm\,s^{-1}}$), increasing the dynamic process has no effect on the final result, but it significantly saves computational resources.

Throughout the movement, the draw cavity was fixed in all directions, while the blank holder and punch could move vertically (z axis), these movements are shown in Figure 6. To eliminate the clearance, the blank holder moves 1 mm in the first 0.005 s to make the contact with the workpiece. Therefore, the punch moves uniformly all the time to make contact with the blank after clamping.

The stamping-drawing process continued until the part failed structurally.

2.6. PERFORMING CALCULATIONS

During the calculation, the energy balance was controlled (Figure 7). It should be noted that the deformation energy (internal energy) and the contact energy (contact energy) start to increase at the time $t = 0.068$ s, after the contact between the punch and the workpiece (Figures 7, point 3 and 8c), until this moment, at $t = 0.025$ s, the blank holder comes into contact with the workpiece (Figures 7, point 1 and 8a), then, at $t = 0.05$ s, the workpiece is pressed into the draw cavity (Figures 7, point 2 and 8b). Then, from point 3 to 5, there is the stamping-drawing process (the view of the workpiece at the intermediate point 4 is shown in Figure 8d).

At point 5, the material failure begins in the area where the bottom joins the wall (Figure 8e), which is indicated by the appearance energy of structural failure (Eroded Internal Energy) and the bottom completely fractures at point 6 (Figures 7 and 8f).

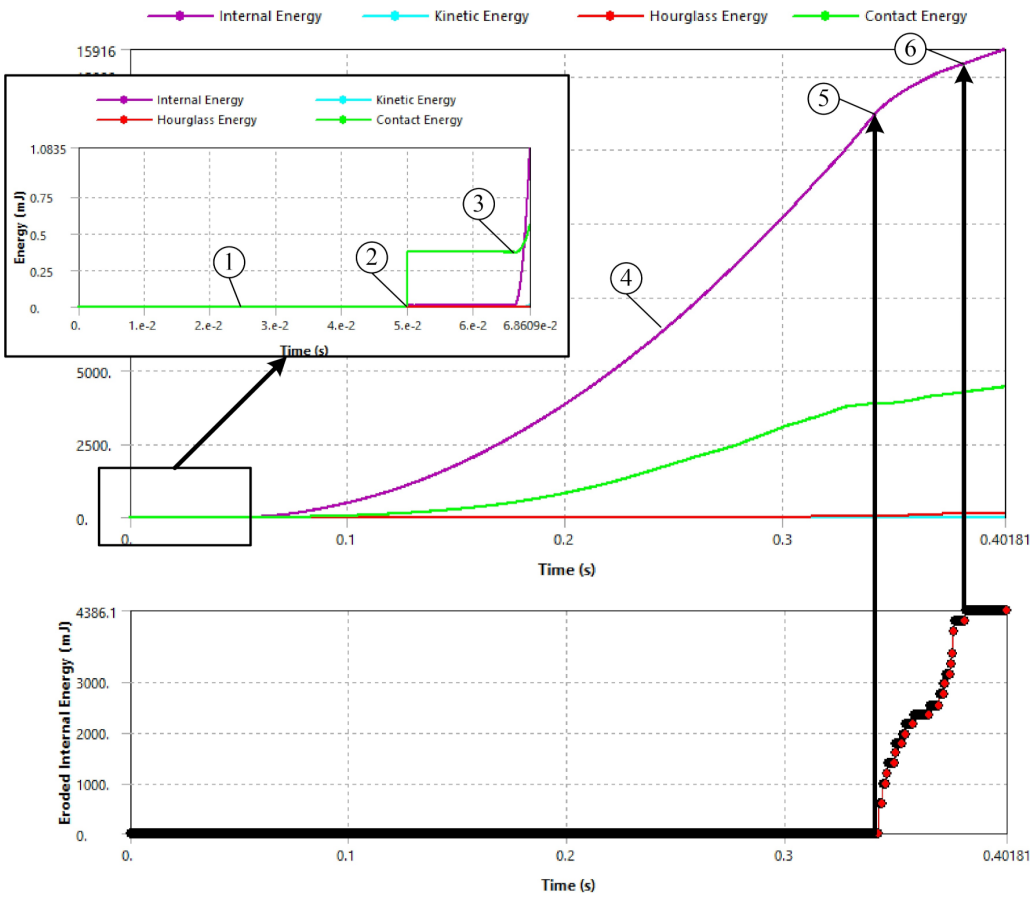

Figure 7. Energy balance.

3. Materials and experimental study

3.1. Material properties

More recently, sheet metals have included aluminium alloys, titanium alloys, and magnesium alloys. Among these, aluminium alloys are the most widely used in mechanical industries due to their low cost and good formability. The selection of materials for the study was based not only on the distribution of materials in the aerospace industry, but also in general mechanical engineering. Therefore, blanks of three aluminium alloys AMg (Al-Mg), AMc (Al-Mn) and D16T (Al-Cu-Mg), and one titanium alloy OT4(Ti-Al-Mn), whose chemical compositions are shown in Table 2, were made for the experimental study.

3.2. Test setup

The experiments were conducted in the Aircraft Engine Power Plant Production Technologies department Laboratory of National Aerospace University in Kharkiv, using modified laboratory hydraulic press P-125. Experiments have been carried out on stamping-drawing experimental setup as shown in Figure 9. The equipment for carrying out the stamping-drawing experiments consists of a die (die corner is 3 mm), punches (diameters are 28 mm and 57 mm for 100 mm sheet), blank holder, a power source (hydraulic power source) for applying the punching force, and instrumentation for measuring the load (pressure gauge). The stamping-drawing experiments have been performed on 1 mm thick sheet metal specimens. Thus, to provide the contact pressure, the die with the blank holder is held stationary, while the punch is moved by the hydraulic press. The blank holding pressure was kept at $1\,\mathrm{N\,mm^{-2}}$ and $2\,\mathrm{N\,mm^{-2}}$ by three bolt connections with load adjustment using a torque wrench; the average punch speed has been kept at $3\,\mathrm{mm\,s^{-1}}$. We have increased the number of results obtained and added an additional workpiece size compared to a previous study [35]. In particular, stamping-drawing have been performed with different workpiece diameters (47 mm, 52 mm, 63 mm and 100 mm), as shown in Figure 10.

The drawing process was carried out with an adjustable drawing die (see Figure 9); the breaking load was set using a calibrated pressure gauge. In order to simulate the contact conditions of an industrial metal stamping-drawing process, the surfaces of the sheets were kept as delivered, i.e. the aluminium blanks were cut from dry lubricated sheets and titanium alloys under dry conditions. Due to the fact that titanium and its alloys belong to the materials, which are very difficult to process by cold metal forming, especially by sheet metal forming, the processing conditions have been changed. Therefore, in order to achieve the desired high quality of the finished titanium part,

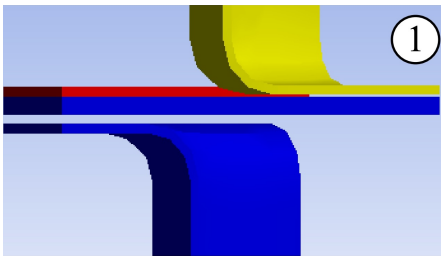

(A). The blank holder come into contact with the workpiece.

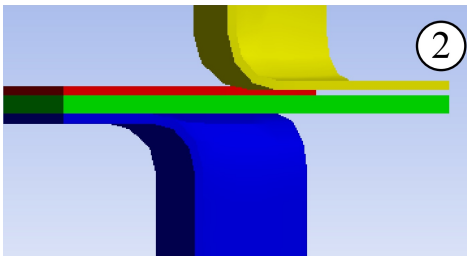

(B). The workpiece is pressed into the draw cavity.

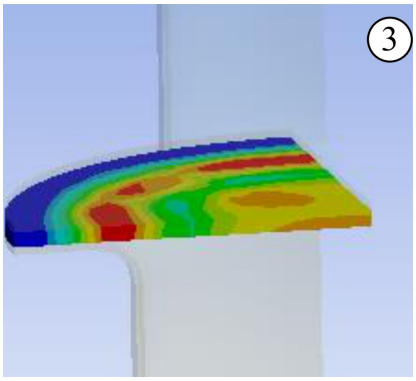

(C). The view of the workpiece at the initial moment.

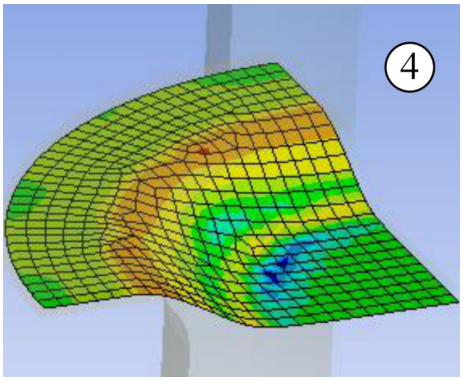

(D). The view of the workpiece at the intermediate point.

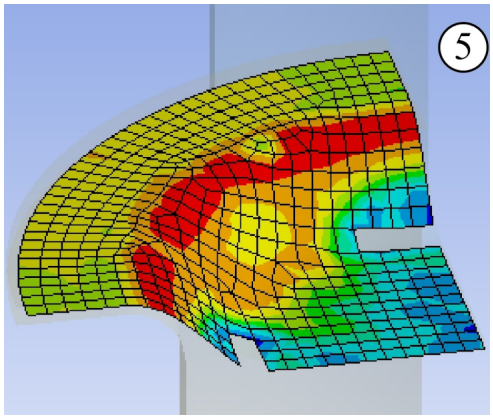

(E). The material failure beginning.

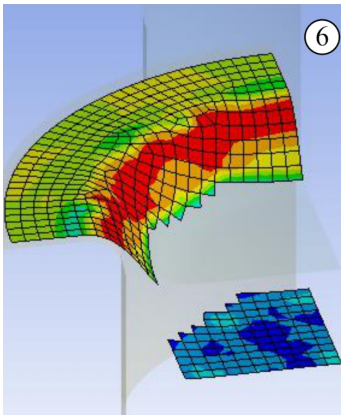

(F). The bottom completely fractures.

FIGURE 8. The stamping-drawing process (deformation and structural failure of the part).

(A). Hydraulic press machine.

(B). Stamping-Drawing die.

FIGURE 9. Stamping-Drawing experimental setup.

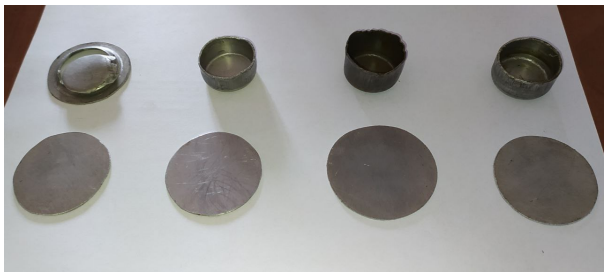

Figure 10. Parts after breaking load (force).

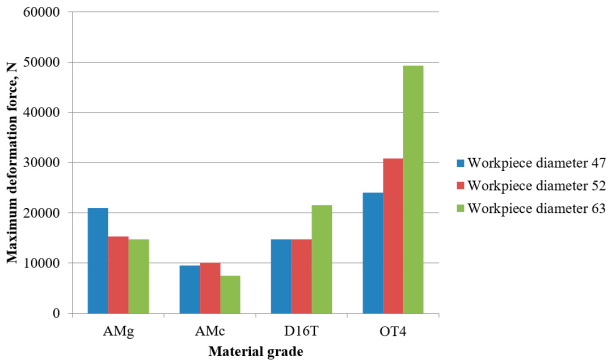

Figure 11. Drawing force for various blanks.

it is necessary to change the nominal contact pressure compared to aluminium alloys. So, two nominal contact pressures were considered, $1\,\mathrm{N\,mm^{-2}}$ for aluminium alloys and $2\,\mathrm{N\,mm^{-2}}$ for titanium alloys. These values represent typical process conditions in stamping-drawing of aluminium and titanium alloy sheets.

Figure 11 shows the dependency of the maximum drawing load of workpieces for three standard material sizes. All workpieces with a diameter of 100 mm, except titanium, were material failures during sheet metal stamping-drawing processes, and therefore this part of the study was not included in the diagram.

It is observed that the drawing load for medium strength and high ductility Al alloys such as (AMg (Al-Mg) and AMc (Al-Mn)) decreases as the workpiece diameter increases. However, for D16T (Al-Cu-Mg) and titanium alloy OT4 (Ti-Al-Mn), a continuous increase was obtained with increasing diameter of the blanks. This is due to high yield strength and strength of D16T (Al-Cu-Mg) and OT4 (Ti-Al-Mn) alloys. It can be seen that the structural failure of workpieces AMg (Al-Mg) and AMc (Al-Mn) occurs faster for diameters of 63 mm. In addition most structural failures occur almost at the beginning of the deformation process at the bottom [35].

Note that the deformation process for ductile aluminium alloys is similar to the punching process. The predicted test results also show that stronger alloys have significantly greater deformations before failure, requiring more effort.

4. Theoretical model

4.1. Previous research results

This theoretical research is based on the previous contribution in the proceedings [35]. In order to calculate of the deformation cell, the continuity hypothesis is required, the main goal of flow kinematics being the determination of the particle velocity field. Furthermore, the significant forces of internal friction allow the metal particles to rotate in the deformation region, therefore, this movement cannot be considered as potential. Hence, the particle velocity in four-dimensional space can be defined by a velocity vector:

$$V = v_x i + v_y j + v_z k + v_t n. \tag{1}$$

In addition, the volume constancy and particles rotating during the deformation are given by system of equations [36]:

$$\left.\begin{aligned} \mathrm{div}V &= 0, \\ \mathrm{rot}V &\neq 0. \end{aligned}\right\} \tag{2}$$

Using Equations (1) and (2), we can determine the particle velocity field of the material, which makes it possible to calculate the strain rates, components of deformation, and to find the energy-power process parameters. It is well known that the, die corner is a part of the torus that can be described by a system of parametric equations [35]:

$$\left.\begin{aligned} x(t,\phi) &= R + r\cos(\omega t)\cos(\omega t), \\ y(t,\phi) &= R + r\cos(\omega t)\sin(\omega t), \\ z(t,\phi) &= \pm r\sin(\omega t), \end{aligned}\right\} \tag{3}$$

where

r is the radius of the die corner,

R is the distance from the rotation axis of the torus to the axis of the generatrix,

t is the time of deformation,

ω is constant (see Figure 12).

After differentiating the system of Equation (3) in time and transforming to Euler coordinates, we obtain a system of equations describing the velocity field of metal displacements at the die corner.

Thus, the velocity field of the metal flow in the deformation zone has the following form:

$$\left.\begin{aligned} V_\rho(\rho) &= -\frac{V_0}{r}\sqrt{r^2-(\rho-R)^2}, \\ V_z(z) &= -\frac{V_0}{r}\sqrt{r^2-z^2}, \\ V_\psi(\rho,\psi,z) &= \left[\frac{V_0\left[r^2-(R-\rho)(R-2\rho)\right]}{r\sqrt{r^2-(\rho-R)^2}} - \frac{V_0 z\rho}{r\sqrt{r^2-z^2}}\right]\psi. \end{aligned}\right\} \tag{4}$$

4.2. Calculating a strain rates and deformations

The strain rate during the stamping-drawing process is an important parameter that is frequently used to characterise plastic flow [37, 38].

In particular, the displacement velocity field (Equation (4)) of the material particles allows the determination of strain rates, defined as:

$$\begin{aligned}
\epsilon_{\rho\rho} &= \frac{\delta V_\rho}{\delta\rho},\\
\epsilon_{\psi\psi} &= \frac{1}{\rho}\frac{\delta V_\psi}{\delta\psi} + \frac{V_\rho}{\rho},\\
\epsilon_{zz} &= \frac{\delta V_z}{\delta z},\\
\epsilon_{\psi z} &= \frac{1}{\rho}\frac{\delta V_z}{\delta\psi} + \frac{\delta V_\psi}{\delta z},\\
\epsilon_{\rho\psi} &= \frac{\delta V_\psi}{\delta\rho} - \frac{V_\psi}{\rho} + \frac{1}{\rho}\frac{\delta V_\rho}{\delta\psi},\\
\epsilon_{\rho z} &= \frac{\delta V_\rho}{\delta z} + \frac{\delta V_z}{\delta\rho} = 0.
\end{aligned} \tag{5}$$

Using Equation (4) and performing the actions indicated in Equation (5), we can be obtain:

$$\begin{aligned}
\epsilon_{\rho\rho} =& -\frac{V_0\left(2R-2\rho\right)}{2r\sqrt{r^2-\left(R-\rho\right)^2}},\\
\epsilon_{\psi\psi} =& -\frac{\frac{V_0\left[(R-\rho)(R-2\rho)-r^2\right]}{r\sqrt{r^2-(R-\rho)^2}} + \frac{V_0\rho z}{r\sqrt{r^2-z^2}}}{\rho}\\
&-\frac{V_0\sqrt{r^2-\left(R-\rho\right)^2}}{\rho r},\\
\epsilon_{zz} =& \frac{V_0 z}{r\sqrt{r^2-z^2}},\\
\epsilon_{\psi z} =& -\psi\left[\frac{V_0\rho}{r\sqrt{r^2-z^2}} + \frac{V_0\rho z^2}{r\left(r^2-z^2\right)^{\frac{3}{2}}}\right],\\
\epsilon_{\rho\psi} =& \psi\left[\frac{V_0\left(3R-4\rho\right)}{r\sqrt{r^2-\left(R-\rho\right)^2}} - \frac{V_0 z}{r\sqrt{r^2-z^2}}\right]\\
&+\psi\left[\frac{V_0\left(2R-2\rho\right)\left[\left(R-\rho\right)\left(R-2\rho\right)-r^2\right]}{2r\left[r^2-\left(R-\rho\right)^2\right]^{\frac{3}{2}}}\right]\\
&+\frac{\psi\left[\frac{V_0\left[(R-\rho)(R-2\rho)-r^2\right]}{r\sqrt{r^2-(R-\rho)^2}} + \frac{V_0\rho z}{r\sqrt{r^2-z^2}}\right]}{\rho}.
\end{aligned}$$

The components of deformation are defined as:

$$\begin{aligned}
e_{\rho\rho} =& -\frac{V_0\left(2R-2\rho\right)}{2r\sqrt{r^2-\left(R-\rho\right)^2}}t,\\
e_{\psi\psi} =& -t\frac{\left[\frac{V_0\left[(R-\rho)(R-2\rho)-r^2\right]}{r\sqrt{r^2-(R-\rho)^2}} + \frac{V_0\rho z}{r\sqrt{r^2-z^2}}\right]}{\rho}\\
&-t\frac{V_0\sqrt{R^2-\left(R-\rho\right)^2}}{\rho r},
\end{aligned}$$

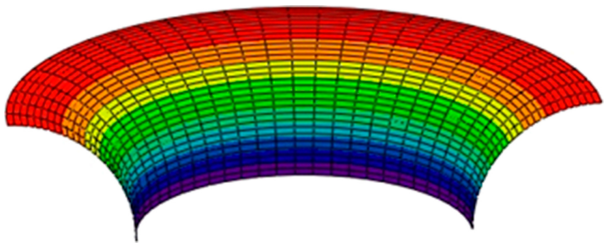

Figure 12. General view of the toroidal surface of die corner [35].

$$\begin{aligned}
e_{zz} =& \frac{V_0 z}{r\sqrt{r^2-z^2}}t,\\
e_{\psi z} =& -\psi\left[\frac{V_0\rho}{r\sqrt{r^2-z^2}} + \frac{V_0\rho z^2}{r\left(r^2-z^2\right)^{\frac{3}{2}}}\right]t,\\
e_{\rho\psi} =& \psi t\left[\frac{V_0\left(3R-4\rho\right)}{r\sqrt{r^2-\left(R-\rho\right)^2}} - \frac{V_0 z}{r\sqrt{r^2-z^2}}\right]\\
&+\psi t\frac{V_0\left(2R-2\rho\right)\left[\left(R-\rho\right)\left(R-2\rho\right)-r^2\right]}{2r\left[r^2-\left(R-\rho\right)^2\right]^{\frac{3}{2}}}\\
&+\frac{\psi\left[\frac{V_0\left[(R-\rho)(R-2\rho)-r^2\right]}{r\sqrt{r^2-(R-\rho)^2}} + \frac{V_0\rho z}{r\sqrt{r^2-z^2}}\right]}{\rho}t.
\end{aligned}$$

In fact, the determination of the stress distribution, which is a function of coordinates and time [39], is one of the main objectives when considering sheet metal stamping operations [40].Thus, mathematical models [41, 42] are necessary to predict power characteristics of various types of stamping. Therefore, it is important for energy-power characteristics to obtain models for calculating the intensity of stresses. The stress intensity has been calculated by the formula:

$$\sigma_i = m\cdot\sigma_t\cdot e_i^n, \tag{6}$$

where

n strain hardening index,

m coefficient taking into account the change in the yield strength of material,

$m\cdot\sigma_t$ flow stress at logarithmic strain $e_i = 1$,

σ_t yield strength [MPa].

5. Validation of the theoretical model by experimental data

According to the usual practice, the results obtained should be analysed with theoretical and experimental data in order to obtain a realistic and accurate model that allows us to evaluate the stamping-drawing process more effectively [43, 44]. The figures of intensity isofields (as mentioned in Figure 13) show the stress obtained as a result of the numerical simulation.

In our opinion, it is interesting to graphically visualise the obtained equations under specific processing conditions. The distribution of the stress intensity

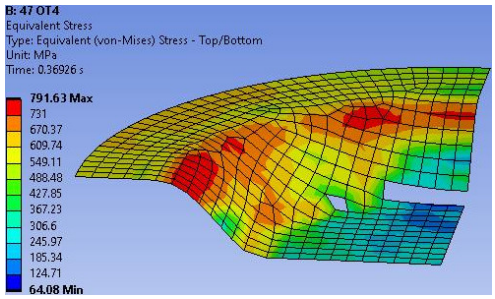

(A). Material grade OT4, time 0.37 s.

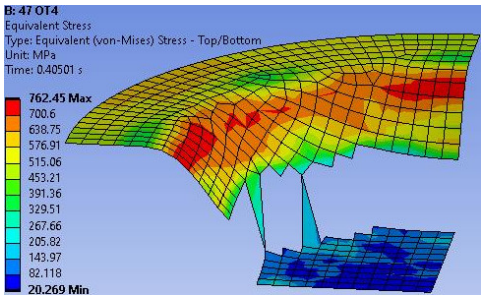

(B). Material grade OT4, time 0.41 s.

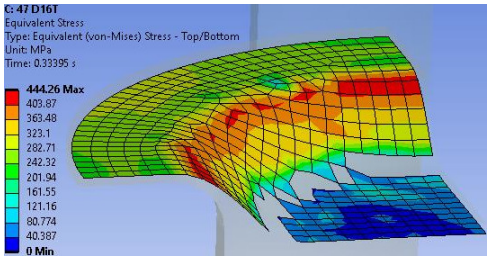

(C). Material grade D16T, time 0.33 s.

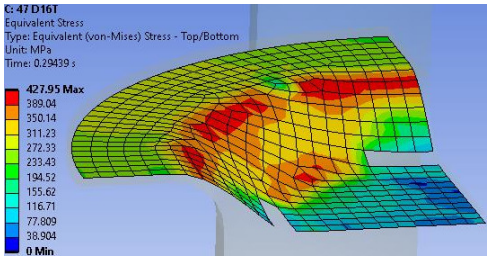

(D). Material grade D16T, time 0.29 s.

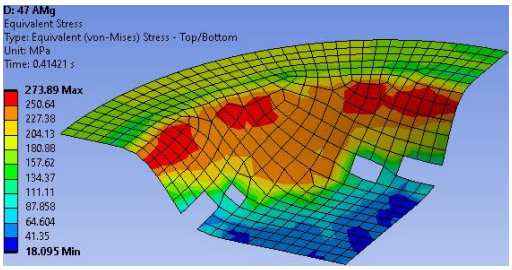

(E). Material grade AMg, time 0.41 s.

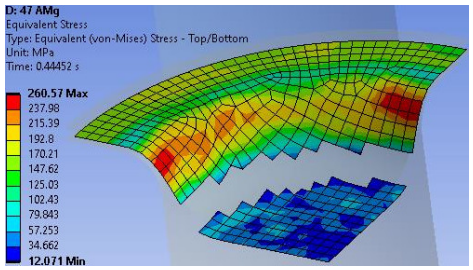

(F). Material grade AMg, time 0.44 s.

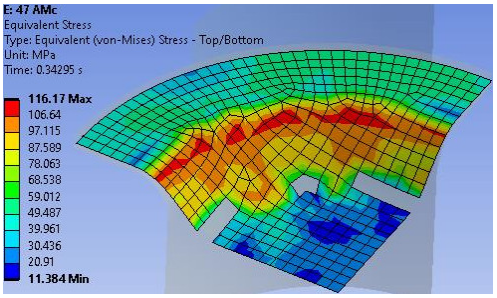

(G). Material grade AMc, time 0.34 s.

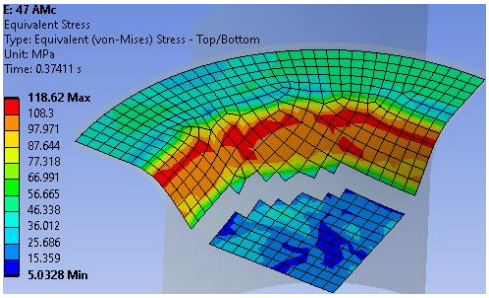

(H). Material grade AMc, time 0.37 s.

Figure 13. Simulated distribution of plastic equivalent stress during stamping-drawing (for different material grade and time of deformation).

during the stamping-drawing process have been plotted (see Figure 14) with the following initial data: $r = 3\,\text{mm}$, $R = 18\,\text{mm}$ and $V = 3\,\text{mm}\,\text{s}^{-1}$; which correspond to the working part diameter matrix of 30 mm and the die corner of 3 mm.

It can be seen that there is a correlation for stress. The predicted stress intensity distributions during the stamping-drawing process are in acceptable agreement with the numerical simulations. As expected, for all investigated materials, the maximum stress values are observed on the die corner. The stresses recorded at the moment of material failure and at the moment of complete separation are slightly different, not exceeding 5 %–10 %. There is a slight decrease in stress at the moment of separation of the bottom, which is explained by the drop load as a result of the facilitation of the stroke of the punch.

The theoretical calculation of the stress intensity was carried out according to Equation (6) from the state of the material isotropy, which made it possible to accept the coincidence of the main axes stressed and deformed states. Therefore, we calculated, the deformation intensities and strain rates for the main linear deformations in order to significantly simplify the stress intensity calculation. Therefore in the model, we have adopted the angular value $\psi = 0$ at the time preceding the structural failure, which corresponds

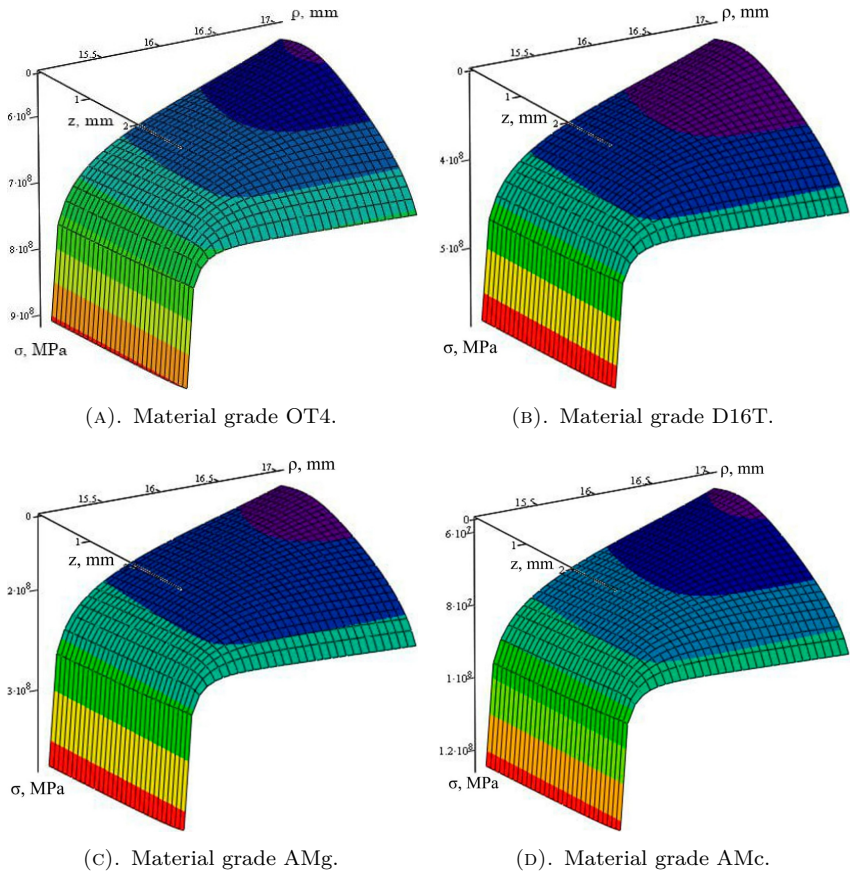

(A). Material grade OT4. (B). Material grade D16T.

(C). Material grade AMg. (D). Material grade AMc.

FIGURE 14. Calculated distribution of stress intensity during stamping-drawing.

to the maximum load. Therefore, we concluded that the theoretical model is acceptable for calculating the entire complex of energy-power characteristics of the stamping-drawing process.

6. CONCLUSION

This research focused on the development of the methodology for calculating the parameters of plastic deformation of metals at the die corner. The stamping-drawing process have been performed with blanks of various diameters (47 mm, 52 mm, 63 mm and 100 mm) for three aluminium and one titanium alloy. From the experimental results, it can be concluded that the forming has demonstrated the dependence of the ultimate stamping-drawing load on the blank diameter. It can be seen that for aluminium ductile alloys, such as AMg (Al-Mg) and AMc (Al-Mn), the drawing load decreases as the workpiece diameter increases. However, aluminium D16T (Al-Cu-Mg) and titanium OT4 (Ti-Al-Mn) alloys have shown a continuous increase in drawing load as the diameter of the blanks increases. This trend suggests a an inverse influence of workpiece diameter on the drawing load for ductile and strong alloys.

In general, we have obtained analytical expressions for the calculation components of strain rates, strains and their intensities. In addition a new approach to calculate the stress intensity at the die corner is presented. The results of the theoretical calculations have been validated by the numerical simulation of the stamping-drawing process in LS-DYNA. It was found that the stresses recorded at the moment of material failure showed good agreement with the simulation, the difference not exceeding 5 %–10 %.

Finally, it can be noted that the theoretical model proposed by us is acceptable for calculating the whole complex of energy-power characteristics of the stamping-drawing process.

ACKNOWLEDGEMENTS

The author acknowledges the support from the project funded by the National Research Foundation of Ukraine, under grant agreement No. 2020.02/0119.

REFERENCES

[1] P. J. Arrazola, T. Özel, D. Umbrello, et al. Recent advances in modelling of metal machining processes. *CIRP Annals* **62**(2):695–718, 2013. https://doi.org/10.1016/j.cirp.2013.05.006

[2] S. Melkote, S. Liang, T. Özel, et al. 100th anniversary issue of the manufacturing engineering division paper. A review of advances in modeling of conventional machining processes: From merchant to the present. *Journal of Manufacturing Science and Engineering* **144**(11):110801, 2022. https://doi.org/10.1115/1.4053522

[3] B. Bahrami, S. Ghouli, M. Nejati, et al. Size effect in true mode II fracturing of rocks: Theory and

experiment. *European Journal of Mechanics – A/Solids* **94**:104593, 2022. https://doi.org/10.1016/j.euromechsol.2022.104593

[4] T. Pepelnjak, L. Sevšek, O. Lužanin, M. Milutinović. Finite element simplifications and simulation reliability in single point incremental forming. *Materials* **15**(10):3707, 2022. https://doi.org/10.3390/ma15103707

[5] A. Graça, G. Vincze. A short review on the finite element method for asymmetric rolling processes. *Metals* **11**(5):762, 2021. https://doi.org/10.3390/met11050762

[6] R. Chitchyan, C. Bird. Theory as a source of software and system requirements. *Requirements Engineering* **27**(3):375–398, 2022. https://doi.org/10.1007/s00766-022-00380-w

[7] G. Martynenko, N. Smetankina, V. Martynenko, et al. Simulation modelling of the process of birds fly into the turbojet aircraft engine fan to determine most dangerous cases in terms of blade strength. In *2022 IEEE 3rd KhPI Week on Advanced Technology (KhPIWeek)*, pp. 1–6. 2022. https://doi.org/10.1109/KhPIWeek57572.2022.9916474

[8] A. Korchagin, Y. Deniskin, I. Pocebneva, O. Vasilyeva. Lean maintenance 4.0: Implementation for aviation industry. In *Transportation Research Procedia*, vol. 63, pp. 1521–1533. 2022. https://doi.org/10.1016/j.trpro.2022.06.164

[9] T. Dolgova, D. Durov, A. Smolyaninov, N. Linkov. Design forming tooling for manufacturing parts from sheet blanks using digital technologies. *E3S Web of Conferences* **376**:01095, 2023. https://doi.org/10.1051/e3sconf/202337601095

[10] V. V. Chigirinsky, Y. S. Kresanov, I. Y. Volokitina. Study of kinematic and deformation parameters of rolling of compressor blade workpieces. *Metallofizika i Noveishie Tekhnologii* **45**(5):631–646, 2023. https://doi.org/10.15407/mfint.45.05.0631

[11] V. Deepak, O. Abhilash, Y. P. Ravitej, et al. Design and development of progressive tool for mold tag. In *AIP Conference Proceedings*, vol. 2316, p. 030015. 2021. https://doi.org/10.1063/5.0038385

[12] H. Kim, J. H. Sung, R. Sivakumar, T. Altan. Evaluation of stamping lubricants using the deep drawing test. *International Journal of Machine Tools and Manufacture* **47**(14):2120–2132, 2007. https://doi.org/10.1016/j.ijmachtools.2007.04.014

[13] E. Evin, N. Daneshjo, A. Mareš, et al. Experimental assessment of friction coefficient in deep drawing and its verification by numerical simulation. *Applied Sciences* **11**(6):2756, 2021. https://doi.org/10.3390/app11062756

[14] M. P. Pereira, M. Weiss, B. F. Rolfe, T. B. Hilditch. The effect of the die radius profile accuracy on wear in sheet metal stamping. *International Journal of Machine Tools and Manufacture* **66**:44–53, 2013. https://doi.org/10.1016/j.ijmachtools.2012.11.001

[15] K. Bouchaâla, M. F. Ghanameh, M. Faqir, et al. Numerical investigation of the effect of punch corner radius and die shoulder radius on the flange earrings for AA1050 and AA1100 aluminum alloys in cylindrical deep drawing process. *Heliyon* **7**(4):e06662, 2021. https://doi.org/10.1016/j.heliyon.2021.e06662

[16] V. M. Brathikan, S. Jayabalu, S. G. Devairakkam, et al. Effect on the product finish in deep drawing process due to supremacy of punch force. In *Journal of Physics: Conference Series*, vol. 2272, p. 012015. IOP Publishing, 2022. https://doi.org/10.1088/1742-6596/2272/1/012015

[17] O. Ozdilli, M. E. Erdin. Comparison of common deep drawing steel sheets in terms of blank holder force and friction conditions. *International Journal of Automotive Science And Technology* **2**(3):36–41, 2018. https://doi.org/10.30939/ijastech..463629

[18] H. Zein, M. El-Sherbiny, M. Abd-Rabou, M. El-Shazly. Effect of die design parameters on thinning of sheet metal in the deep drawing process. *American Journal of Mechanical Engineering* **1**(2):20–29, 2013. https://doi.org/10.12691/ajme-1-2-1

[19] V. M. Brathikan, N. Sangeetha, B. Sangeethkumar, K. Scidarth. Influence of various blank diameter in deep drawing. In *Materials Today: Proceedings*, vol. 68, pp. 1995–1999. 2022. https://doi.org/10.1016/j.matpr.2022.08.281

[20] V. Savas, O. Secgin. A new type of deep drawing die design and experimental results. *Materials & Design* **28**(4):1330–1333, 2007. https://doi.org/10.1016/j.matdes.2006.01.004

[21] P. D. Gogawale, N. Bagal, B. Kedar. Calculation of deep drawing force in CR4 metal forming. *International Journal of Advanced Research in Science & Technology* **8**(3):44–50, 2020. [2024-05-22]. https://ijarsct.co.in/Paper276.pdf

[22] R. Arhat, R. Puzyr, V. Shchetynin, et al. The stress state of the workpiece at the radius of matrix rounding during drawing, considering the bending moment. In V. Tonkonogyi, V. Ivanov, J. Trojanowska, et al. (eds.), *Advanced Manufacturing Processes III*, pp. 479–488. Springer International Publishing, Cham, 2022. https://doi.org/10.1007/978-3-030-91327-4_47

[23] M. Thor, M. G. R. Sause, R. M. Hinterhölzl. Mechanisms of origin and classification of out-of-plane fiber waviness in composite materials – A review. *Journal of Composites Science* **4**(3):130, 2020. https://doi.org/10.3390/jcs4030130

[24] H. Blala, L. Lang, S. Khan, S. Alexandrov. Experimental and numerical investigation of fiber metal laminate forming behavior using a variable blank holder force. *Production Engineering* **14**(4):509–522, 2020. https://doi.org/10.1007/s11740-020-00974-9

[25] S. M. Hussaini, G. Krishna, A. K. Gupta, S. K. Singh. Development of experimental and theoretical forming limit diagrams for warm forming of austenitic stainless steel 316. *Journal of Manufacturing Processes* **18**:151–158, 2015. https://doi.org/10.1016/j.jmapro.2015.03.005

[26] H. Zein, O. M. Irfan. Optimization and mapping of the deep drawing force considering friction combination. *Applied Sciences* **11**(19):9235, 2021. https://doi.org/10.3390/app11199235

[27] Livermore software technology corporation. LS-DYNA® Keyword user's manual. Volume I, 2007. [2024-05-22]. https://www.academia.edu/40555890/LS_DYNA_KEYWORD_USERS_MANUAL_VOLUME_I

[28] ansys.com. Ansys Granta: Materials information management. [2024-05-22]. https://www.ansys.com/products/materials

[29] V. Prakash, D. Ravi Kumar. Numerical simulation of warm deep drawing incorporating strain rate effect in sheet material properties. In *Materials Today: Proceedings*, vol. 18, pp. 2595–2602. 2019. https://doi.org/10.1016/j.matpr.2019.07.118

[30] V. Prakash, R. K. Digavalli, M. Lenzen, et al. Numerical simulation of sheet metal forming of an Al-Mg alloy incorporating plane strain properties in the yield criterion. *Proceedings of the Institution of Mechanical Engineers, Part B: Journal of Engineering Manufacture* **238**(3):373–384, 2024. https://doi.org/10.1177/09544054221135388

[31] J. Domitner, Z. Silvayeh, A. Shafiee Sabet, et al. Characterization of wear and friction between tool steel and aluminum alloys in sheet forming at room temperature. *Journal of Manufacturing Processes* **64**:774–784, 2021. https://doi.org/10.1016/j.jmapro.2021.02.007

[32] A. Gontarz, A. Dziubińska, Ł. Okoń. Determination of friction coefficients at elevated temperatures for some Al, Mg and Ti alloys. *Archives of Metallurgy and Materials* **56**(2):379–384, 2011. https://doi.org/10.2478/v10172-011-0040-x

[33] M. D. Sharma, R. Sehgal. Dry sliding friction and wear behaviour of titanium alloy (Ti-6Al-4V). *Tribology Online* **7**(2):87–95, 2012. https://doi.org/10.2474/trol.7.87

[34] J. Adamus, P. Lacki, M. Motyka, K. Kubiak. Investigation of sheet-titanium drawability. In *Proceedings of the 12th World Conference on Titanium*, pp. 337–340. 2012.

[35] A. Onopchenko, O. Horbachov, V. Sorokin, et al. Optimal conditions for deformation of stamping-drawing process from aviation materials. In V. Tonkonogyi, V. Ivanov, J. Trojanowska, et al. (eds.), *Advanced Manufacturing Processes IV*, pp. 109–118. Springer International Publishing, Cham, Germany, 2023. https://doi.org/10.1007/978-3-031-16651-8_11

[36] M. O. Kurin. Analysis the process of plastic deformation metal chip at non-free cutting. *Metallofizika i Noveishie Tekhnologii* **42**(3):433–449, 2020. https://doi.org/10.15407/mfint.42.03.0433

[37] Y. P. Korkolis, B. R. Mitchell, M. R. Locke, B. L. Kinsey. Plastic flow and anisotropy of a low-carbon steel over a range of strain-rates. *International Journal of Impact Engineering* **121**:157–171, 2018. https://doi.org/10.1016/j.ijimpeng.2018.07.015

[38] D. Sánchez-Ávila, R. Barea, E. Martínez, et al. Determination of the instantaneous strain rate during small punch testing of 316L stainless steel. *International Journal of Mechanical Sciences* **149**:93–100, 2018. https://doi.org/10.1016/j.ijmecsci.2018.09.042

[39] T.-T. Luyen, V.-C. Tong, D.-T. Nguyen. A simulation and experimental study on the deep drawing process of SPCC sheet using the graphical method. *Alexandria Engineering Journal* **61**(3):2472–2483, 2022. https://doi.org/10.1016/j.aej.2021.07.009

[40] A. Singh, S. Basak, P. S. Lin Prakash, et al. Prediction of earing defect and deep drawing behavior of commercially pure titanium sheets using CPB06 anisotropy yield theory. *Journal of Manufacturing Processes* **33**:256–267, 2018. https://doi.org/10.1016/j.jmapro.2018.05.003

[41] M. Mahmoud, F. Bay, D. P. Muñoz. An efficient multiphysics solid shell based finite element approach for modeling thin sheet metal forming processes. *Finite Elements in Analysis and Design* **198**:103645, 2022. https://doi.org/10.1016/j.finel.2021.103645

[42] R. K. Lal, V. K. Choubey, J. P. Dwivedi, S. Kumar. Study of factors affecting springback in sheet metal forming and deep drawing process. In *Materials Today: Proceedings*, vol. 5, 2, pp. 4353–4358. 2018. https://doi.org/10.1016/j.matpr.2017.12.002

[43] N. Fang, I. S. Jawahir. Analytical predictions and experimental validation of cutting force ratio, chip thickness, and chip back-flow angle in restricted contact machining using the universal slip-line model. *International Journal of Machine Tools and Manufacture* **42**(6):681–694, 2002. https://doi.org/10.1016/S0890-6955(02)00006-8

[44] D. Sornette, A. B. Davis, K. Ide, et al. Algorithm for model validation: Theory and applications. In *Proceedings of the National Academy of Sciences*, vol. 104, 16, pp. 6562–6567. 2007. https://doi.org/10.1073/pnas.0611677104